Published in final edited form as:
Ultrasound Med Biol. 2012 November ; 38(11): 2031–2037. doi:10.1016/j.ultrasmedbio.2012.06.011.

ON THE ADVANTAGES OF IMAGING THE AXIAL-SHEAR STRAIN COMPONENT OF THE TOTAL SHEAR STRAIN IN BREAST TUMORS

Arun K. Thittai[1], **Belfor Galaz**[1,2], and **Jonathan Ophir**[1]

[1]The University of Texas Medical School, Department of Diagnostic and Interventional Imaging, Ultrasonics and Elastographics Laboratory, Houston, Texas, USA

[2]Universidad de Santiago de Chile (USACH), Department of Physics, Santiago, Chile

Abstract

Axial-shear strain elastography was described recently as a method to visualize the state of bonding at an inclusion boundary. Although total shear strain elastography was initially proposed for this purpose, it did not evolve beyond the initial reported Finite Element Model (FEM) and Simulation studies. One of the major reasons for this was the practical limitation in estimating the tissue motion perpendicular (lateral) to the ultrasound (US) beam as accurately as the motion along the US beam (axial). Nevertheless, there has been a sustained effort in developing methods to improve the lateral motion tracking accuracy and thereby obtain better quality total shear strain elastogram (TSSE). We hypothesize that in some cases, even if good quality TSSE becomes possible, it may still be advantageous to utilize only the axial-shear strain (one of the components of the total shear strain) elastogram (ASSE). Specifically, we show through FEM and corroborating tissue-mimicking gelatin phantom experiments that the unique "*fill-in*" discriminant feature that was introduced recently for asymmetric breast lesion classification is depicted *only* in the ASSE and not in the TSSE. Note that the presence or conspicuous absence of this feature in ASSE was shown to characterize asymmetric inclusion s' boundaries as either loosely-bonded or firmly-bonded to the surrounding, respectively. This might be an important observation because the literature suggests that benign breast lesions tend to be loosely-bonded, while malignant tumors are usually firmly-bonded. The results from the current study demonstrate that the use of shear strain lesion "*fill-in*" as a discriminant feature in the differentiation between asymmetric malignant and benign breast lesions is only possible when using the ASSEs and not the TSSEs.

Keywords

Axial-shear strain; Asymmetric lesion; Benign; Bonding; Breast cancer; Discriminant feature; Elastography; Elliptical; FEM; Fibroadenoma; Malignant; Orientation; Shear Strain Fill-in; Sonogram; Total Shear Strain; Ultrasound

Contact: Arun K. Thittai, PHD, The University of Texas Medical School, Department of Diagnostic and Interventional Imaging, Ultrasonics Laboratory, 6431 Fannin St., Houston, TX 77030, USA, 713.500.7651 Direct, 713.500.7694 Fax, Arun.K.Thittai@uth.tmc.edu.

INTRODUCTION

Ultrasound (US) elastography (Ophir et al. 1991) is now a well-established technique, which has been incorporated into many commercial ultrasound scanners used in clinical practice. This technique involves acquiring US (RF/envelope) signals from an imaging plane in tissue before and after a small applied quasi-static compression and computing all the local axial displacements in the imaging plane. The gradients of these displacements are then used to generate a map of the local axial strains in the tissue. This strain map is referred to as an *axial strain elastogram* (Ophir et al. 1999).

Based on the axial strain elastograms alone, elastography has been shown to be helpful in a wide variety of clinical applications such as in detecting tumors in breast and prostate tissues (Céspedes et al. 1993; Garra et al. 1997; Hiltawski et al. 2001; Lorenz et al. 1999), monitoring HIFU therapy in the prostate (Souchon et al. 2003), thyroid tumor classification (Lyshchik et al. 2005; Bae et al. 2007), lymph node characterization (Săftoiu et al. 2006), monitoring thermal ablation (Kallel et al. 1999, Righetti et al. 1999; Bharat et al. 2005; Souchon et al. 2005), and in intravascular plaque characterization (de Korte et al. 2000). The utility of elastography for the reduction of the rate of unnecessary breast biopsies has recently been demonstrated by Regner et al. (2004), Svensson et al. (2005), Barr (2006) and Burnside et al. (2007). It is reasonable to assume that any additional independent mechanical tissue parameters that can be imaged with elastography may either improve current elastographic performance and / or find utility in newer applications.

We have shown that in addition to the axial strain, which is one of the strain tensors that describe the target deformation, it is feasible to image another strain tensor in the form of the axial-shear strain (Thitaikumar et al. 2007). We have demonstrated that the axial-shear strain distribution pattern around an inclusion is directly influenced by the bonding at the inclusion-background boundary using simulations, gelatin-phantom experiments, and breast lesions *in vivo* (Thitaikumar et al. 2007). Results from an initial study to evaluate the potential of axial-shear strain elastograms (ASSEs) to differentiate between fibroadenomas (reported to be loosely-bonded to their host tissue (cf. Fry 1951)) and cancers (reported to be firmly-bonded to the surrounding tissue (cf. Fry 1951)) in the breast have been very promising (Thitaikumar et al. 2008, 2011). The earlier work on ASSEs had assumed a simple, circularly-symmetric inclusions. More recent papers have corroborated our original reports on the utility of ASSE for breast lesion classification using this inclusion model (Xu et al. 2010, Varghese 2011).

Recently, we extended the simple circularly-symmetric inclusion model to a more general elliptical geometry with an arbitrary orientation with respect to the axis of compression. For ease of description, we will refer to this more general model as “asymmetric inclusion model”. With this generalization, we have shown that finite, non-zero, interior axial-shear strains were present only in “loosely-bonded” asymmetric inclusions. This phenomenon was referred to as “*fill-in*” (Galaz et al. 2009, Thittai et al. 2010)*. The presence or absence of this “*fill-in*” was shown as a potential easily-recognizable feature that could distinguish benign fibroadenomas from malignant breast lesions (Thittai et al. 2010). Our original observation on the presence of “*fill-in*” only in the loosely-bonded, asymmetric inclusion model, and its conspicuous absence in the firmly-bonded asymmetric inclusion was independently corroborated and reported recently (figure 3 in Xu et al. 2011).

It should be noted that almost all of the work discussed in the preceding paragraph focuses on estimating and imaging the local distribution of **axial-shear strain** (the 1st term of

*Please note that Thitaikumar and Thittai refer to the same author who had a name change recently.

equation 1 below) in an elastically inhomogeneous material. The total shear strain is defined as the sum of the axial- and lateral-shear strain components (both terms in eqn. 1), where (*u, v*) are the lateral and axial displacement components along the *x*- and *y*-axes, respectively (Timoshenko and Goodier 1970).

$$\varepsilon_{x,y}=\frac{1}{2}\left(\frac{\partial v}{\partial x}+\frac{\partial u}{\partial y}\right) \quad (1)$$

The ability to use the total shear strain ($\varepsilon_{x,y}$) for assessing the inclusion bonding properties was first shown through finite element simulation and US simulation studies more than a decade ago (Konofagou et al. 2000). Later, it was shown that using only the axial component $(\frac{\partial v}{\partial x})$ of the total shear strain had a practical advantage in terms of superior image quality (ThitaiKumar et al. 2005). This is due to the well-known US limitation that the estimation of motion *along* the direction of the US beam axis is significantly more precise than estimation of the motion *across* the US beam axis. Therefore, the relatively inferior image quality of the lateral component estimate $(\frac{\partial u}{\partial y})$ was seen as the primary *practical* reason for developing ASSE (ThitaiKumar et al. 2006, 2007, 2007a, 2008, 2011, Chen et al., 2010, Garcia et al. 2011, Xu et al. 2010, Varghese 2011).

Moreover, we report in this paper that in certain cases it may be *necessary* to use the axial shear strain image for *fundamental* reasons. This is because important unambiguous features that are present in the shear strain components (axial- or lateral- component alone) may be completely absent in the total shear strain image. Specifically, we demonstrate below through simple Finite Element Modeling (FEM) and tissue-mimicking gelatin phantom experiments that the "*fill-in*" discriminant feature (Galaz et al. 2009, Thittai et al. 2010) can be imaged and utilized only by using the ASSE and not the total shear strain elastogram (TSSE).

In addition to the above demonstration, we also show in this paper that the inclusion "*fill-in*" that is visualized in ASSE can be interpreted effectively as an image of rotation, which is defined by Timoshenko and Goodier (1970) as

$$\omega_{x,y}(\text{rotation})=\frac{1}{2}\left(\frac{\partial v}{\partial x}-\frac{\partial u}{\partial y}\right) \quad (2)$$

Note that unlike the total shear strain defined in Eq. 1, the difference between the two components defines the rotation.

MATERIALS AND METHODS

Finite Element Modeling

A 2D plane strain model was built by using the finite-element modeling (FEM) software ANSYS® (Ansys Inc, Canonsburg, PA) in a manner similar to what was described in our previous papers (Galaz et al. 2009, Thitaikumar et al. 2007). Briefly, the geometry consisted of a single stiff elliptical inclusion embedded in a homogenous, softer background with overall dimensions of 40 mm by 40 mm. The centroid of the inclusion was placed at the center of lateral axis of symmetry and the long axis of the inclusion was oriented at 45° axially. The FEM phantom was meshed with quadrilateral elements of 8 nodes, 4 nodes at the corners of the quadrilateral and 1 more node at the mid-point of each side. These

elements are preferred for plane strain problems (Young and Budynas 2002). The Young's modulus values of the inclusion and background were set to of 42 kPa and 21 kPa, respectively. A constant Poisson's ratio value of 0.495 was set for the inclusion and the background materials to model essentially incompressible conditions.

By default, the degree of bonding at the inclusion-background boundary was modeled as being firmly-bonded by the FEM software. However, the FEM software allows the users to define contact elements and assign a coefficient of friction (μ) at the inclusion-background boundary to simulate varying degrees of bonding (Thitaikumar et al. 2007). In that paper we showed that μ values close to 0 simulate loosely-bonded boundary condition, whereas when μ approaches 1 the strain patterns start to resemble that of firmly-bonded boundary condition. For the purposes of this study, we created a loosely-bonded inclusion by assigning μ=0.01. The model was subjected to a uniaxial compressive strain of 1% by loading it from the top. The node at the axis of lateral symmetry at the bottom of the model was confined in the axial and lateral direction to avoid any rigid motion of the whole model. The pre- and post-compression node coordinate positions were saved and processed in MATLAB® (Mathworks, MA) to compute the axial-shear strain, lateral-shear strain, total shear strain and the rotation images.

Phantom Experiment

In order to corroborate the FEM predictions, we utilized previously-acquired experimental data from tissue mimicking phantom studies (Thittai et al. 2010). Specifically, we utilized the data obtained from an elastographic experiment performed on "Phantom 4" (Loosely bonded inclusion: phantom height=80 mm, width=80 mm, $\theta \sim 45°$)). The readers are referred to the reference for detailed description of the phantom preparation and experimental set up.

Data Acquisition

A Sonix 500-RP (Ultrasonix Medical Corporation, BC, Canada) ultrasound scanner, with a 128-element linear array, 10-MHz center frequency was used for data acquisition. The radio-frequency (RF) sampling rate was 40 MHz. The transducer was attached to a compressor plate (80 × 40 mm), which was in turn attached to a precision computer-driven digital motion controller (Chandrasekhar et al. 2006). The phantom was submerged in water during imaging. The phantom was compressed from the top by a small amount that corresponded to an applied strain of 1%. Pre- and post-compression RF data sets were acquired from the phantom at 10 different planes along the elevational direction. The planes were separated by at least 3 mm (~elevational beamwidth) to obtain independent frames for subsequent averaging. The ASSEs, Lateral-shear strain elastograms (LSSE) and TSSEs were obtained from the experimental data using the algorithm described briefly below.

Displacement tracking and ASSE, LSSE, and TSSE generation

The displacement tracking algorithm consisted of a multilevel, coarse-to-fine, 2-D block-matching scheme similar to those presented in the literature (Zhou and Hall 2002; Shi and Varghese 2007; Lopata et al. 2009). The principal difference was the use of the sum square difference (SSD) similarity measure in the coarse level on the envelope of the signal, followed by the cross-correlation (CC) measure on the RF signal in the fine level around the SSD-tracked coarse displacement region. This algorithm was described along with a flow chart in Thittai et al. (2010). Readers are referred to that paper for a detailed description. After obtaining the axial displacement using the 2-D tracking method, the ASSE was generated by extending the staggered strain estimation originally proposed by Srinivasan et al. (2002) for axial strain estimation. In the extended version, the axial displacements are staggered along the lateral direction to estimate the axial–shear strain (ThitaiKumar et al.

2007). Similarly, the LSSE was generated by staggering the lateral displacements along the axial direction. The total SSE was obtained as the sum ASSE and LSSE and scaled by a factor of ½ (see Eqn. 1). The rotation elastogram was obtained using Eqn 2.

RESULTS

FEM

Figure 1 compares the images of the axial- and lateral- components of the total shear strain as predicted by the FEM. The total shear strain obtained as half the sum of these two components is also shown. Note that finite, non-zero axial- and lateral- shear strains, referred to previously as "*fill-in*", are visible inside the inclusion in the axial-shear strain and lateral-shear strain images, respectively. Interestingly, the opposite polarities of the two components cancel each other out such that there is no observable "*fill-in*" in the total shear strain image. As opposed to the total shear strain image, the axial- and lateral-shear strains reinforce each other to yield finite non-zero values inside the rotation image. It is easy to observe that the rotation image resembles the axial-shear strain image with only very slight differences in the strain pattern outside the inclusion. Also, note the presence of a thin ring of high strain values along the inclusion boundary in all cases.

Phantom experiments

Figure 2 compares the ASSE, LSSE and TSSE obtained from the phantom experiment. As expected, observe that the LSSE is of appreciably inferior image quality compared to the ASSE. However, despite this limitation, "*fill-in*" can be visualized only in the ASSE and the LSSE and is essentially absent in the TSSE, as predicted by the FEM results. Also, note that the rotation elastogram has finite values inside the inclusion and resembles the ASSE although it is visibly much noisier.

Apart from the "*fill-in*" effect, we also observe the presence of a thin, high-contrast axial-shear and lateral-shear strain zone that has opposite polarity of that of the values inside the inclusion in the experimental elastograms. This is in part due to the finite resolution effects of the ultrasound system and partly due to a physical separation (a thin gap of finite dimension) that exists between the inclusion and background which is created during the manufacture of loosely-bonded condition. These reasons are similar to those that were thoroughly investigated and reported earlier (ThitaiKumar et al. 2007).

DISCUSSION

It is clear from the results that in the case of loosely-bonded asymmetric inclusions the "*fill-in*" feature is present only in the images of the axial-and lateral- component of the shear strain and not in the total shear strain image. This is an important observation as it suggests that in some clinical cases where observing the "*fill-in*" is important for tumor classification, imaging only one of the components may be fundamentally advantageous to imaging the total shear strain. Additionally, given that the axial-shear strain is of superior image quality compared to the lateral-component (see Fig 2), the results from this paper demonstrate the advantage of using only the ASSE compared to LSSE or TSSE.

Moreover, the images of rotation shown (figure 1d and 2d) add a very interesting interpretation of the "*fill-in*" observed in the ASSEs. It is clear from figure 1c and 2c that the total shear strain inside the inclusion is zero and therefore Eqn. 1 yields $\frac{\partial v}{\partial x} = -\frac{\partial u}{\partial y}$. Using this relationship in Eqn. 2 it becomes clear that $w_{x,y}(\text{rotation}) = \frac{\partial v}{\partial x}$, which is the axial-shear

strain component. In other words, it can be said that it is the rotation and not the total shear strain which has useful information about whether the inclusion is bonded or not. This makes intuitive sense, i.e., a bonded lesion cannot rotate, nor would a loosely-bonded symmetric lesion. Only loosely-bonded asymmetric lesion would rotate. ASSE essentially provides this information, but is much superior in image quality compared to rotation image that is nosier due to computation involving the lateral-shear strain component.

There has been a sustained effort to develop algorithms to improve the quality of lateral-displacement motion tracking for elastography over the years (cf. Konofagou et al. 1998, Tanter et al. 2002, Techavipoo et al. 2004, Jiang and Hall 2010). The interest has been to obtain better quality lateral displacement estimates that will in turn result in better quality estimates of lateral-shear strain and thereby total shear strain (cf. Konofagou et al. 1998, 2000, Techavipoo et al. 2004, Jiang and Hall 2010). In a recent report, Xu et al. (2011) compare the ASSE and TSSE (which is referred to as full-shear strain in their paper) through FEM and phantom experiments. They corroborate our previous findings that unique "*fill-in*" feature in ASSE is present only for loosely-bonded, non-normally oriented (w.r.t axis of compression), elliptical inclusion and not for firmly-bonded inclusion (see Figure 3 in Xu. et al. 2011). However, one may notice that the ASSE and TSSE reported in Xu et al (2011) look almost identical. Also, the total-shear strain pattern shown in figure 3 in Xu et al. (2011) for firmly-bonded inclusion at normal orientation (0°) is different from the total-shear strain image published by the same group previously (figure 7 in Rao et al. 2007) and others (figure 2.2 in ThitaiKumar 2007), although it was for circular inclusions.

While it is important to sustain efforts in the above direction, this paper shows that there are cases where utilizing only one component may offer unique benefits. Specifically, the results from the current study demonstrate that the use of "*fill-in*" as a feature in the identifying inclusion boundary condition as either loosely-bonded or firmly-bonded is possible using *only* the ASSEs and not the TSSEs. This is an important observation because the literature suggests that benign breast lesions tend to be loosely-bonded, while malignant tumors are usually firmly-bonded (Fornage et al. 1984).

CONCLUSIONS

In this paper, we have shown using an FEM and tissue-mimicking gelatin phantom experiments that the dramatic occurrence of *fill-in* is observable only in the ASSE and not in the total shear strain image. The results confirm that not only it is advantageous to use ASSE, which is one of the components of total shear strain, but it may be the *only* quality image that can exploit the 'presence' or 'absence' of *fill-in* to assess the bonding conditions of asymmetric inclusions.

Acknowledgments

This work was supported in part by NIH grant R21-CA135580-01 and by the John S. Dunn foundation. The authors would like to thank the anonymous reviewers for their valuable comments and suggestions that improved the paper.

REFERENCES

Bae U, Dighe M, Dubinsky T, Minoshima S, Shamdasani V, Kim Y. Ultrasound thyroid elastography using carotid artery pulsation: preliminary study. J Ultrasound Med. 2007; 26:797–805. [PubMed: 17526611]

Barr, RG. Clinical applications of a real time elastography technique in breast imaging; Proc 5th Int Conf Ultrasonic Measurement and Imaging of Tissue Elasticity; 2006. p. 112

Bharat S, Techavipoo U, Kiss M, Liu W, Varghese T. Monitoring stiffness changes in lesions after radiofrequency ablation at different temperatures and durations of ablation. Ultrasound Med Biol. 2005; 31:415–422. [PubMed: 15749565]

Burnside ES, Hall TJ, Sommer AM, Hesley GK, Sisney GA, Svensson WE, Fine JP, Jiang J, Hangiandreou NJ. Differentiating benign from malignant solid breast masses with US strain imaging. Radiology. 2007; 245(2):401–410. [PubMed: 17940302]

Céspedes I, Ophir J, Ponnekanti H, Maklad N. Elastography: elasticity imaging using ultrasound with application to muscle and breast *in vivo*. Ultrasonic imaging. 1993; 15:73–88. [PubMed: 8346612]

de Korte C, Pasterkamp G, van der Steen AFW, Woutman HA, Bom N. Characterization of plaque components with intravascular ultrasound elastography in human femoral and coronary arteries *in vitro*. Circulation. 2000; 102:617–623. [PubMed: 10931800]

Fornage BD, Lorigan JG, Andry E. Fibroadenoma of the breast: Sonographic appearance. Radiology. 1989; 172:671–675. [PubMed: 2549564]

Fry KE. Benign lesions of the breast. CA Cancer J Clin. 1951; 4:160–161.

Galaz, B.; ThitaiKumar, A.; Ophir, J. Axial-shear strain distributions in an elliptical inclusion model (part I): A simulation study. Proc of the 8th International Conference on Ultrasonic Measurement of Imaging of Tissue Elasticity; Vlissingen, Zeeland, Netherlands. 2009. p. 99

Garcia, L.; Bamber, JC.; Fromageau, J.; Uff, C. Can ultrasound elastography differentiate between a thin layer of soft tissue and slippery boundary?. Proc. of the 10th International Conference on Ultrasonic Measurement of Imaging of Tissue Elasticity; Arlington, Texas, USA. 2011. p. 78

Garra BS, Céspedes I, Ophir J, Spratt SR, Zuurbier RA. Elastography of breast lesions: initial clinical results. Radiology. 1997; 202:79–86. [PubMed: 8988195]

Hiltawski KK, Kruger M, Starke C, Heuser L, Ermert H, Jensen A. Freehand ultrasound elastography of breast lesions: Clinical results. Ultras Med Biol. 2001; 27(11):1461–1469.

Jiang, J.; Hall, TJ. A coupled speckle tracking algorithm for elasticity imaging: initial in vivo experience. Proc. of the 9th International Conference on Ultrasonic Measurement of Imaging of Tissue Elasticity, Snow Bird; Utah, USA. 2010. p. 74

Kallel F, Stafford RJ, Price RE, Righetti R, Ophir J, Hazle JD. The Feasibility of Elastographic Visualization of HIFU-Induced Thermal Lesions in Soft-Tissue. Ultras. Med. and Biol. 1999; 25(4):641–647.

Konofagou EE, Ophir J. A new elastographic method for estimation and imaging of lateral displacements, lateral strains, corrected axial strains and Poisson's ratio in tissues. Ultrasound in Med Biol. 1998; 24(8):1183–1199. [PubMed: 9833588]

Konofagou EE, Harrigan T, Ophir J. Shear strain estimation and lesion mobility assessment in elastography. Ultrasonics. 2000; 38:400–404. [PubMed: 10829696]

Lopata RGP, Nillesen MM, Hansen HHG, Gerrits IH, Thijssen JM, De Korte CL. Performance evaluation of methods for two-dimensional displacement and strain estimation using ultrasound radio frequency data. Ultrasound Med Biol. 2009; 35:1580–1591.

Lorenz A, Sommerfeld HJ, Schurmann MG, Philippous S, Senge T, Ermert H. A new system for the acquisition of ultrasonic multicompression strain images of the human prostate in vivo. IEEE Trans Ultrason Ferroelec Freq Cont. 1999; 46(5):1147–1154.

Chen L, Housden RJ, Treece GM, Gee AH, Prager RW. A Normalization Method for Axial- Shear Strain Elastography. IEEE Trans Ultrason Ferroelec Freq Cont. 2012; 57(12):2833–2838.

Lyshchik A, Higashi T, Asato R, Tanaka S, Ito J, Mai JJ, Pellot-Barakat C, Insana MF, Brill AB, Saga T, Hiraoka M, Togashi K. Thyroid gland tumor diagnosis at US elastography. Radiology. 2005; 237:202–211. [PubMed: 16118150]

Ophir J, Alam SK, Garra BS, Kallel F, Konofagou EE, Krouskop TA, Varghese T. Elastography: Ultrasonic Estimation and Imaging of Elastic Properties of Tissues. Proc Instn Mech Engrs. (UK). 1999; 213(H3):203–233.

Ophir J, Céspedes I, Ponnekanti H, Yazdi Y, Li X. Elastography: a method for imaging the elasticity of biological tissues. Ultrasonic Imaging. 1991; 13(2):11–13.

Rao M, Chen Q, Shi H, Varghese T, Madsen EL, Zagzebski JA, Wilson TA. Normal and shear strain estimation using beam steering on linear-array transducers. Ultrasound Med. Biol. 2007; 33:57–66. [PubMed: 17189047]

Regner DM, Hesley GK, Hangiandreou NJ, Morton MJ, Nordland MR, Meixner DD, Hall TJ, Farrell MA, Mandrekar JN, Harsmen SW, Charboneau JW. Breast lesions: evaluation with US strain imaging—clinical experience of multiple observers. Radiology. 2006; 238:425–437. [PubMed: 16436810]

Righetti R, Kallel F, Stafford RJ, Price RE, Krouskop TA, Hazle JD, Ophir J. Elastographic Characterization of HIFU-induced lesions in canine livers. Ultras Med Biol. 1999; 25(7):1099–1113.

Săftoiu A, Vilmann P, Hassan H, Gorunescu F. Analysis of endoscopic ultrasound elastography used for characterisation and differentiation of benign and malignant lymph nodes. Ultras Med. 2006; 27(6):535–542.

Shi H, Varghese T. Two-dimensional multi-level strain estimation for discontinuous tissue. Phys Med Biol. 2007; 52:389–401. [PubMed: 17202622]

Souchon R, Bouchoux G, Maciejko E, Lafon C, Cathignol D, Bertrand M, Chapelon J. Monitoring the formation of thermal lesions with heat-induced echo-strain imaging: a feasibility study. Ultrasound Med Biol. 2005; 31:251–259. [PubMed: 15708465]

Srinivasan S, Ophir J, Alam SK. Elastographic imaging using staggered strain estimates. Ultrasonic Imaging. 2002; 25:229–245. [PubMed: 12665239]

Svensson, WE.; Amiras, D.; Shousha, S.; Rattansingh, A.; Chopra, D.; Sinnett, HD.; Hall, TJ.; Zhu, Y.; Malin, J.; Lowery, C. Elasticity imaging of 67 cancers and 167 benign breast lesions shows that it could halve biopsy rates of benign lesions; Proc 4th Int Conf Ultrasonic Measurement and Imaging of Tissue Elasticity; 2005. p. 87

Tanter M, Bercoff J, Sandrin L, Fink M. Ultrafast Compound Imaging for 2-D Motion Vector Estimation: Application to Transient Elastography. IEEE Trans. Ultras. Ferro. and Freq. Cont. 2002; 49(10):1363–1374.

Techavipoo U, Varghese T, Zagzebski JA, Chen Q, Liu W. Semiautomated thermal lesion segmentation for three-dimensional elastographic imaging. Ultrasound Med. Biol. 2004; 30:655–664. [PubMed: 15183232]

ThitaiKumar A, Krouskop TA, Garra BS, Ophir J. Visualization of bonding at an inclusion boundary using axial-shear strain elastography: A feasibility study. Phys Med Biol. 2007; 52:2615–2633. [PubMed: 17440256]

Thitalkumar A, Krouskop T, Ophir J. Signal-to-noise ratio, contrast-to-noise ratio, and their tradeoffs with resolution in axial-shear strain elastography. Phys. Med. Biol. 2007a; 52:13–28. [PubMed: 17183125]

Thitaikumar A, Mobbs LM, Kraemer-Chant CM, Garra BS, Ophir J. Breast tumor classification using axial shear strain elastography: a feasibility study. Phys Med Biol. 2008; 53:4809–4823. [PubMed: 18701768]

Thitaikumar A, Righetti R, Krouskop TA, Ophir J. Resolution of axial shear strain elastography. Phys Med Biol. 2006; 51:5245–5257. [PubMed: 17019036]

ThitaiKumar A, Ophir J, Krouskop TA. Noise performance and signal-to-noise ratio of shear strain elastograms. Ultrasonic imaging. 2005; 27:145–165. [PubMed: 16550705]

Thittai AK, Yamal J, Mobbs LM, Kraemer-Chant CM, Chekuri S, Garra BS, Ophir J. Axialshear strain elastography for breast lesion classification: Further *in vivo* results from retrospective data, Ultras. Med and Biol. 2011; 37(2):189–197.

Thittai AK, Galaz B, Ophir J. Axial-shear strain distributions in an elliptical inclusion model: Experimental validation and *in vivo* examples with implications to breast tumor classification, Ultras. Med. Biol. 2010; 36(5):1–7.

Timoshenko, SP.; Goodier, JN. Theory of Elasticity. New York: McGraw-Hill; 1970. p. 8-11.

Varghese T. Erratum: Ultras. Med. Biol. 2011; 37(10):1743.

Xu H, Varghese T, Madsen EL. Analysis of shear strain imaging for classifying breast masses: finite element and phantom results. Med Phys. 2011; 38(11):6119–6127. [PubMed: 22047376]

Xu H, Rao M, Varghese T, Sommer A, Baker S, Hall TJ, Sisney GA, Burnside ES. Axialshear strain imaging for differentiating benign and malignant breast masses. Ultras. Med. Biol. 2010; 36:1813–1824.

Young, WC.; Budynas, RG. Roark's Formulas for Stress and Strain. New York: McGraw-Hill; 2002. p. 76

Zhu Y, Hall TJ. A modified block matching method for real-time freehand strain imaging. Ultrasonic Imaging. 2002; 24:161–176. [PubMed: 12503771]

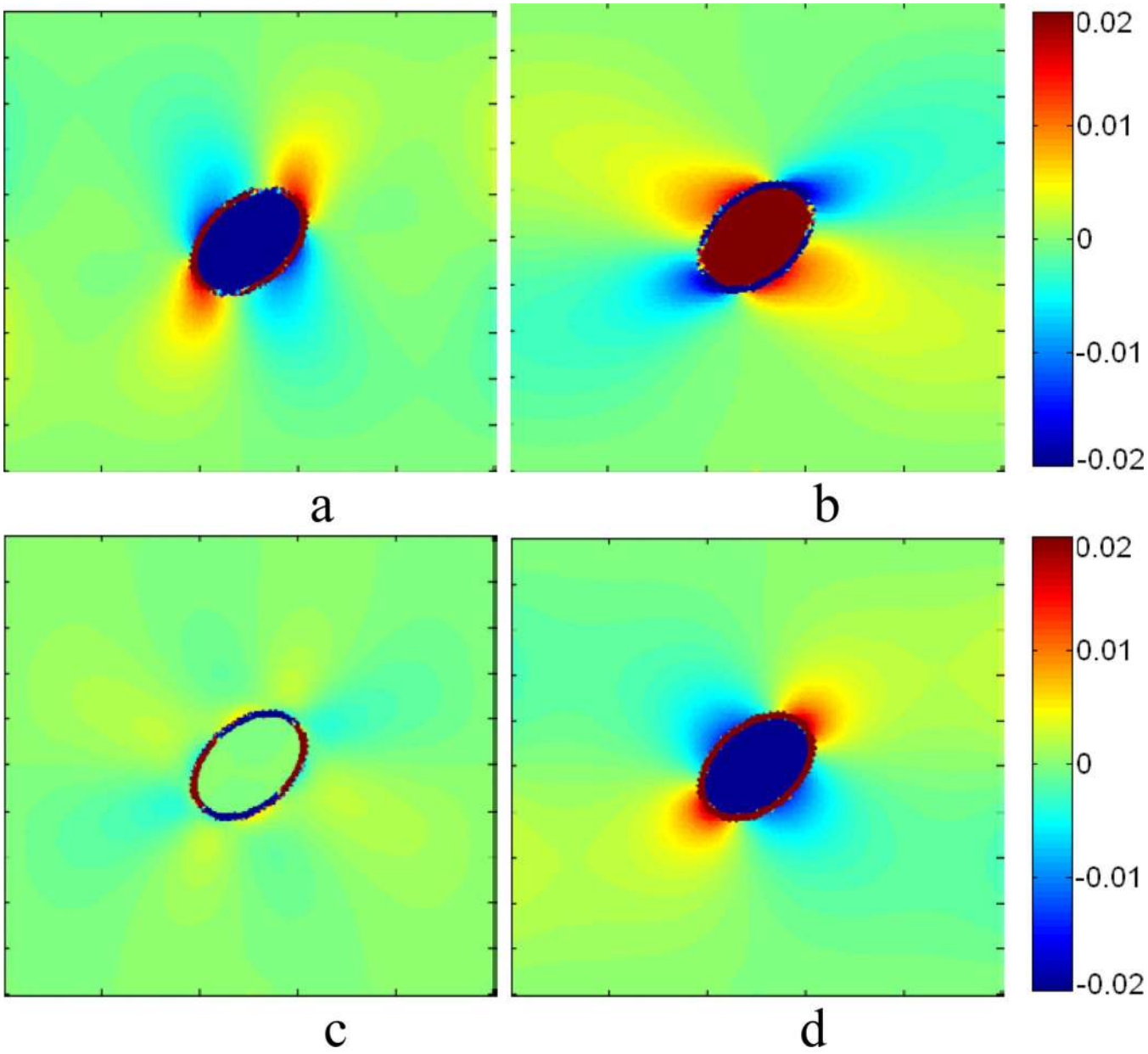

Figure 1.
FEM predictions of (a) Axial-shear strain (b) Lateral-shear strain (c) total shear strain images and (d) Rotation image. Note constant color bar for all three images. The red and the blue color encode the directional polarity of axial-shear strain (blue-negative, red-positive).

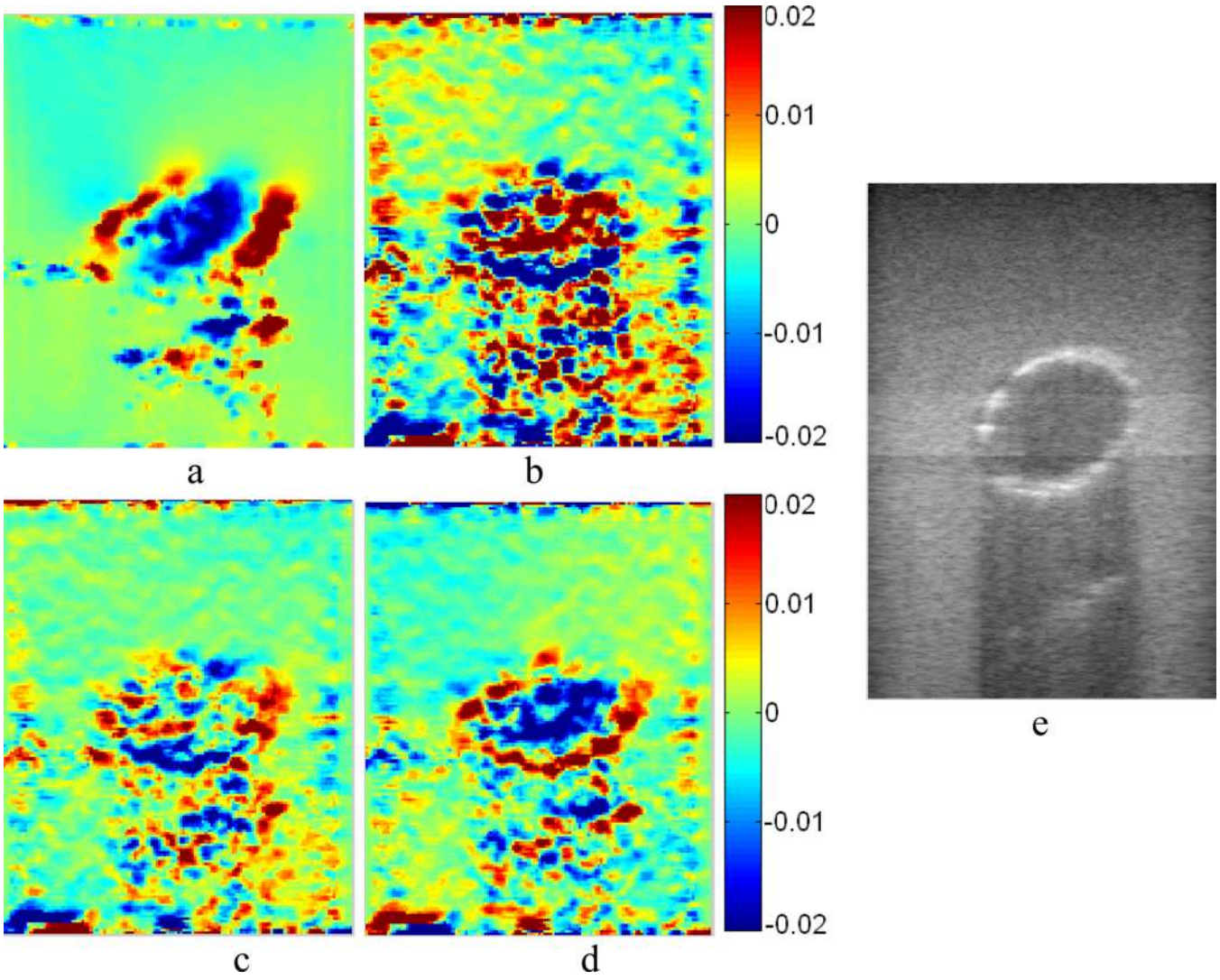

Figure 2.

Elastograms obtained from Phantom experiment of (a) ASSE (b) LSSE (C) TSSE and (d) Rotation elastogram. The corresponding B-mode image of the phantom is provided in (e). Observe the presence of "*fill-in*" in ASSE and not in TSSE. Observe that the image quality of ASSE is appreciably better compared to LSSE or TSSE or rotation elastogram.